Bioactive Materials 6 (2021) 783–793

Contents lists available at ScienceDirect

Bioactive Materials

journal homepage: http://www.keaipublishing.com/biomat

Electrodeposition of calcium phosphate onto polyethylene terephthalate artificial ligament enhances graft-bone integration after anterior cruciate ligament reconstruction

Jiangyu Cai[a,1], Qianqian Zhang[b,1], Jiebo Chen[a], Jia Jiang[a], Xiumei Mo[b], Chuanglong He[b,*], Jinzhong Zhao[a,**]

[a] Department of Sports Medicine, Shanghai Jiao Tong University Affiliated Sixth People's Hospital, Shanghai, 200233, China
[b] State Key Laboratory for Modification of Chemical Fibers and Polymer Materials, College of Chemistry, Chemical Engineering and Biotechnology, Donghua University, Shanghai, 201620, China

ARTICLE INFO

Keywords:
Electrodeposition
Calcium-phosphate
Graft-bone integration
Polyethylene terephthalate
Artificial ligament

ABSTRACT

It is a big challenge to develop a polyethylene terephthalate (PET) artificial ligament with excellent osteogenetic activity to enhance graft-bone integration for ligament reconstruction. Herein, we evaluated the effect of biomineralization (BM) and electrodeposition (ED) method for depositing calcium-phosphate (CaP) on the PET artificial ligament *in vitro* and *in vivo*. Scanning electron microscopy and energy-dispersive X-Ray spectrometer mapping analysis revealed that the ED-CaP had more uniform particles and element distribution (Ca, P and O), and thermogravimetric analysis showed there were more CaP on the PET/ED-CaP than the PET/BM-CaP scaffold. Moreover, the hydrophilicity of PET scaffolds was significantly improved after CaP deposition. *In vitro* study showed that CaP coating via BM or ED method could improve the attachment and proliferation of MC3T3-E1 cells, and ED-CaP coating significantly increased osteogenic differentiation of the cells, in which the Wnt/β-catenin signaling pathway might be involved. In addition, radiological, histological and immunohistochemical results of *in vivo* study in a rabbit anterior cruciate ligament (ACL) reconstruction model demonstrated that the PET/BM-CaP and PET/ED-CaP scaffolds significantly improved graft-bone integration process compared to the PET scaffold. More importantly, larger areas of new bone ingrowth and the formation of fibrocartilage tissue were observed at 12 weeks in the PET/ED-CaP group, and the biomechanical tests showed increased ultimate failure load and stiffness in PET/ED-CaP group compared to PET/BM-CaP and PET group. Therefore, ED of CaP is an effective strategy for the modification of PET artificial ligament and can enhance graft-bone integration both *in vitro* and *in vivo*.

1. Introduction

Anterior cruciate ligament (ACL) rupture is a common injury in professional sports as well as recreation, and reconstructive surgery of the injured ligament using autologous, allogeneic or artificial graft is often needed. Autologous graft is the most common choice for surgeons. However, it may cause pain, weakness and altered biomechanics at the harvest site [1]. The advantages of allogeneic graft are no donor site morbidity, a shorter operation time and less painful initial recovery. Nevertheless, it has the risk of disease transmission, bacterial infection, and the possibility of allergic reactions [2,3]. To avoid drawbacks of the autologous and allogeneic grafts, there has been an increasing interest on the application of artificial ligament in the clinical practice [4]. Although some biodegradable materials such as silk, polylactic-co-glycolic acid, polylactic acid and polycaprolactone have been used for tendon/ligament engineering in the basic research, there remains difficulties in their transformation from basic to clinical application [5–9]. The Ligament Advanced Reinforcement System (LARS), made of polyethylene terephthalate (PET), one kind of non-degradable materials, is the most commonly used artificial ligament for ACL reconstruction, and

Peer review under responsibility of KeAi Communications Co., Ltd.
* Corresponding author.
** Corresponding author. Department of Sports Medicine, Shanghai Jiao Tong University Affiliated Sixth People's Hospital/Shanghai Sixth People's Hospital, 600 Yishan Road, Shanghai, 200233, China.
E-mail addresses: hcl@dhu.edu.cn (C. He), jzzhao@sjtu.edu.cn (J. Zhao).
[1] Both authors contributed equally to this work.

https://doi.org/10.1016/j.bioactmat.2020.08.037
Received 13 July 2020; Received in revised form 3 August 2020; Accepted 17 August 2020

it is also the only one approved by China Food and Drug Administration for clinical use in China. Due to its excellent mechanical property, LARS ligament enables a fast recovery with satisfactory short-term and mid-term outcomes after surgery [10]. Nevertheless, the hydrophobic property of PET makes it difficult for cell adhesion and tissue ingrowth, and thus result in poor graft-bone healing and relatively high rate of graft failure in the long-term follow-up [11].

Generally, ligament-to-bone insertions can be divided into two categories: indirect and direct types [12]. The indirect type consists of three zones including ligament, Sharpey's fibers and bone. The Sharpey's fibers extend from ligament tissue into bone tissue. The direct type, such as the insertion of the ACL, comprises four zones: ligament, unmineralized fibrocartilage, mineralized fibrocartilage and bone tissues. The highly specialized fibrocartilage structure is essential for minimizing stress concentrations and mediating load transfer between the soft and hard tissues [13]. Therefore, an ideal repair is to establish a biomimetic conjunction between the graft and the host bone. However, it is difficult to achieve effective interface healing in direct type due to the complexity of the transition between ligament and bone tissues [14].

In recent years, surface modification has been applied to PET in order to improve its biological performance and to further enhance the integration between PET and host bone [15]. Previous studies have used various bioactive substances such as graphene, CaP and bioactive glass for surface modification on PET [16–18]. Among them, calcium-phosphate (CaP) is characterized by excellent osteoinductivity and biocompatibility and has been applied to enhance bone ingrowth across the interface between graft and host bone. However, according to the histological findings of the previous studies [17,19,20], there was still fibrous scar tissue band instead of fibrocartilage structure at the graft−bone interface, which was far from the result of an ideal reconstruction. Some technical factors, such as the amount and homogeneity of the CaP coating, remained unknown, which may be associated with the imperfect results. Our previous studies have used electrodeposition (ED) as an approach to deposit apatite coatings onto the electrospinning scaffolds [21,22]. It was proved to be an effective method to realize rapid mineralization with uniform deposition matrices. However, to date, few studies have reported the effect of ED of CaP onto the PET scaffold for artificial ligament application.

The aim of this study is to evaluate the effect of ED method against the conventional biomineralization (BM) method in depositing CaP on PET artificial ligament *in vitro* and *in vivo*. The effect of CaP coating on cellular viability and function were assessed using the MC3T3-E1 mouse pre-osteoblast cell. Furthermore, an animal study was also performed to evaluate the effect of PET/ED-CaP ligament in a rabbit ACL reconstruction model. It is hypothesized that ED is a more effective strategy for depositing CaP on PET artificial ligament than the BM method and can enhance graft-bone integration *in vitro* and *in vivo*.

2. Materials and methods

2.1. Preparation of PET/BM-CaP and PET/ED-CaP

The PET sheets (4 cm × 4 cm) were kindly provided by MicroPort Scientific Corporation (Shanghai, China) and were fabricated according to our previous study [23]. The PET sheets were cleaned in the 75% (v/v) alcohol solution for 4 h, and then washed with deionized water. For the PET/BM-CaP group, the PET sheet was treated with ammonia water and then immersed in the Ca–P solution (0.042 M $Ca(NO_3)_2{\cdot}4H_2O$ and 0.025 M $NH_4H_2PO_4$) at 37 °C for 24 h. The pH value was adjusted to 7.4 using $NH_3{\cdot}H_2O$ and HCl. Subsequently, the sheet was washed with deionized water and dried at room temperature. For the PET/ED-CaP group, ED was performed in an electrolyte containing 0.042 M $Ca(NO_3)_2{\cdot}4H_2O$ and 0.025 M $NH_4H_2PO_4$, and the pH value was adjusted to 4.8 by $NH_3{\cdot}H_2O$ and HCl. A two-electrode electrochemical system was applied for ED. The PET sheet, pretreated with ammonia water, was immobilized onto the surface of stainless-steel electrode as the working electrode, while a platinum plate electrode used as the counter electrode and a saturated calomel electrode as the reference electrode. The deposition voltage, time and temperature in the ED process were fixed at 3 V, 2 h and 37 °C. After ED, the PET/ED-CaP sheet was rinsed with deionized water and then dried at room temperature. The PET, PET/BM-CaP and PET/ED-CaP sheets were cut into round slices with a diameter of 1.4 cm for *in vitro* study. The sheets and the slices were sterilized by ethylene oxide prior to *in vitro* or *in vivo* experiments.

2.2. Characterization

The morphology of PET, PET/BM-CaP and PET/ED-CaP sheets was observed by scanning electron microscopy (SEM) at 10 kV (Hitachi TM-1000, Japan). Chemical elemental analysis of CaP coated on the surface of PET sheet was detected by energy-dispersive X-Ray spectrometer (EDS, Bruker, German). The thermogravimetric analysis (TGA) was performed to measure the quantity of CaP in the PET/BM-CaP and the PET/ED-CaP groups using on a Pyris 1 thermogravimetric analyzer (PerkinElmer, USA). The TGA data of the samples were recorded under air atmosphere at a scan rate of 10 °C min^{-1} from 50 °C to 700 °C. Besides, surface hydrophilicity of samples was detected by water contact angle (WCA, JC200C1, Zhongchen Co., Shanghai, China). Images of droplets were recorded through image analyzer to measure the contact angles.

2.3. In vitro experiments

2.3.1. Cell seeding and cytocompatibility tests

The preosteoblast cell lines (MC3T3-E1) were purchased from the Type Culture Collection of Chinese Academy of Sciences (Shanghai, China). The MC3T3-E1 cells were seeded on the PET, PET/BM-CaP and PET/ED-CaP slices in a density of 1×10^5 cells per well with alpha-minimum essential medium (α-MEM, Gibco, USA) containing 10% fetal bovine serum (Gibco, USA) as well as 1% penicillin and streptomycin solution (Gibco, USA) in 24 well plates. In order to avoid the influence of the cells leaking into the bottom of the plate, the slices with adhesive cells were transferred into new 24-well plates after 24 h culture according to the protocol of our previous study [24]. The culture medium was refreshed every other day. After 1 and 5 days of culture, the culture medium was removed and the samples were washed with PBS for three times. For cell morphology study, the samples were fixed by 2.5% glutaraldehyde for 2 h and dehydrated with graded ethanol. Subsequently, the samples were sputtered with gold for 30s twice at a current of 8 mA and the morphology of cells was observed by SEM.

For cell viability analysis, LIVE/DEAD Viability/Cytotoxicity Kit (Mesgen biotech, Shanghai, China) were used according to the manufacturer's instruction. A fluorescence microscope (Olympus Corporation, Tokyo, Japan) was used to capture the images. Three randomly-chosen fields of view were photographed from each sample. Four samples yielded 12 photos for each scaffold after 1 or 5 days of culture. To quantitatively evaluate the cell viability at each time point, the area of live cells attaching to the sample was divided by the total area to obtain: Live cell area per total area = $Area_{live}/Area_{total}$.

Besides, cell counting kit-8 (CCK-8) assay was used to evaluate cell proliferation after 1, 3 and 5 days of culture. At each time point, the culture medium was removed and the cultured cells were washed with PBS twice. Then, 360 μL of the fresh culture medium and 40 μL of CCK-8 solution (Mesgen biotech, Shanghai, China) were added to each well and reacted for 4 h in the incubator. A total of 100 μL of supernatant was transferred to a 96-well plate, and the absorbance was measured at 450 nm with a microplate reader (Multiskan FC, Waltham, MA, USA).

2.3.2. Alkaline phosphatase (ALP) activity

The MC3T3-E1 cells were seeded on the different slices in 24-well plates at a density of 1×10^5 cells per well and cultured in osteogenic

induction medium for 7 and 14 days. At each time point, ALP staining was performed using a 5-bromo-4-chloro-3-indolyl phosphate/nitro-bluetetrazoli (BCIP/NBT) Alkaline Phosphatase Color Development Kit (Beyotime, Shanghai, China) according to the manufacturer's protocol. Semiquantitative analysis of ALP activity was performed by using the ALP assay kit (Beyotime, Shanghai, China). In brief, the cells were lysed in 300 μL of 0.2% Triton X-100, followed by sonication and centrifugation at 13 000 rpm for 15 min at 4 °C. The supernatant was collected to measure the ALP activity according to the protocol of the ALP assay kit. Meanwhile, the total protein content of each sample was calculated using a Bicinchoninic Acid (BCA) protein assay kit (Beyotime, Shanghai, China). The ALP ability was normalized against the total protein content and described as nmol/min/mg total protein.

2.3.3. Alizarin red S (ARS) staining

ARS (Sigma-Aldrich, Germany) staining was used as an indicator of bone-nodule formation. The MC3T3-E1 cells were seeded onto on the different slices in 24-well plates an at a density of 1×10^5 cells per well and cultured in osteogenic induction medium for 21 and 28 days. At each time point, cells were washed with PBS and fixed with 2.5% glutaraldehyde in PBS buffer for 4 h at 4 °C. Then, the cells were washed with distilled water and stained with 20 mg/mL ARS (pH 4.2) for 30 min at room temperature and washed with PBS until there was no ARS dye in the water. For quantification of the staining of each sample, 10% (w/v) cetylpyridinium chloride (Sigma) was used and the optical density value of the dye concentration was measured at 562 nm.

2.3.4. RT-qPCR

Total RNA was extracted from the cells cultured in the different sheets by TRIzol (Invitrogen, Carlsbad, CA, USA) after 7 and 14 days of culture. The cDNA was generated using oligo-dT primers (oligo-dT primers (Promega, USA)) according to the manufacturer's protocol. Quantitative PCR was performed with SYBR Green Premix Ex Taq (Takara, Kyoto, Japan) and then detected by using an RT-PCR system (Takara, Kyoto, Japan). The expression of target genes (ALP, COL1, osteocalcin (OCN) and osteopontin (OPN) were normalized against β-actin. Relative gene expression values were calculated by $2^{-\Delta\Delta Ct}$ method. The primers for RT-qPCR were described in Table S1.

2.3.5. Western blot

To investigate the underlying mechanism of the scaffolds for osteogenic differentiation of MC3T3-E1 cells, after 7 days of culture, cells were lysed with ice-cold RIPA (Thermo Fisher Scientific) and the total proteins were extracted. BCA protein assay kit (Beyotime, Shanghai, China) was used to measure the concentration of total protein. Protein samples (20 μg) were subjected to electrophoresis on 12% sodium dodecyl sulfate-polyacrylamide gels and electrotransferred onto polyvinylidene fluoride membranes (Millipore Corp., Bedford, MA) at 4 °C for 2 h. Then the membranes were blotted using 5% Carnation nonfat dry milk and incubated with anti-collagen I antibody, *anti*-osteopontin antibody, *anti*-Wnt-5a antibody, *anti*-β-catenin antibody and *anti*-β-actin antibody (all purchased from Abcam, Inc., Cambridge, MA) overnight at 4 °C, respectively. The membranes were washed with phosphate-buffered saline containing 0.1% (v/v) Tween-20 and incubated with horseradish peroxidase (HRP)-conjugated secondary antibodies for 2 h. After extensive washing, immunoreactive proteins were visualized using the enhanced chemiluminescence reagent (Thermo Fisher Scientific, Rockford, IL, USA) and were quantitatively analyzed with Quantity-One analysis software (Bio-Rad, Munich, Germany).

2.4. In vivo experiments

2.4.1. ACL reconstruction animal model

Animal experiments procedures were approved by the Animal Research Committee of Shanghai Jiao Tong University Animal Science Department. Sixty New Zealand rabbits with a mean weight of 3.0 ± 0.5 kg were randomly divided to three groups: PET group (n = 20), PET/BM-CaP group (n = 20) and PET/ED-CaP group (n = 20). The PET sheets were cut into the size of 4 cm × 1 cm and rolled up into ligament with a diameter of 0.25 cm for *in vivo* implantation. The ACL reconstruction was performed under strictly aseptic conditions. The rabbits were anesthetized by intramuscular injection of 0.8 mL of xylazine hydrochloride and 0.8 mL of diazepam, and one of the knees was randomly selected for ACL reconstruction. A medial parapatellar incision was made, and the patella was dislocated laterally. The native ACL was exposed and sharply dissected from the insertion sites. The bone tunnels were drilled with a 0.25 cm-diameter Kirschner wire in the femoral and tibial insertion sites of the native ACL. The artificial ligament was then passed from the tibial bone tunnel to the femoral bone tunnel. Both ends of the grafts were sutured to the adjacent periosteum and soft tissue with a 3–0 Ethibond suture (Johnson & Johnson, New Brunswick, NJ, USA). The wound was closed layer by layer. The animals were returned to cages without immobility and the penicillin was injected into them intramuscularly with 100,000 U/kg for consecutive 3 days after surgery. The rabbits were sacrificed at 6 and 12 weeks and the femur-graft-tibia complex samples were harvested for the Micro-CT analysis, histological and immunohistochemical assessment and biomechanical test (Table S2).

2.4.2. Micro-CT analysis

At 12 weeks after surgery, the samples were scanned at a spatial resolution of 35 μm (1 mm aluminum filter, 65 KV, 380 μA) via Skyscan 1176 micro-CT imaging system (Bruker, Kontich, Belgium). The Data Viewer, CTvol and CTAn were analyzed to calculate the average cross-sectional area of the bone tunnel. Moreover, the bone volume fraction (BV/TV value), which means the fraction of a given volume of interest that is occupied by mineralized bone, was also measured. The higher BV/TV value indicated the better graft-bone integration in our study.

2.4.3. Histological and immunohistochemical assessment

The samples were fixed in 10% formalin for 48 h, and were then decalcified with 10% ethylene diaminete traacetic acid for 8 weeks. After dehydration in a graded series of ethanol and embedment in paraffin, the samples were sectioned with a thickness of 5 mm perpendicular to the longitudinal axis of the graft and stained with hematoxylin eosin (H&E), Masson trichrome and toluidine blue (TB). Slides were observed using an inverted light microscopy (IX71SBF-2, Olympus Co., Tokyo, Japan), and digital images were captured using a DP Manager (Olympus Optical Co. Ltd.). To semi-quantify the histological results, the slides were evaluated by two independent observers who were blinded as to the group and time point of the samples according to a modified score system (Table S3) [6,25]. Furthermore, immunohistochemical staining was performed to detect the expression of collagen I, collagen II, OPN, Wnt-5a and β-catenin at 12 weeks after surgery. Sections were incubated with the associated primary antibody overnight at 4 °C and with the associated secondary antibody for 1 h at 37 °C. Then, the tissues in the sections were developed in DAB solution (Dako, Hamburg, Germany) with counterstaining in hematoxylin.

2.4.4. Biomechanical test

Immediately after sacrifice, the samples were harvested from each knee and prepared for mechanical testing. All the sutures and soft tissues except for the ACL graft, were carefully removed from the samples. The femoral and tibial bone were immobilized firmly in clamps and biomechanical test was carried out using an Instron tensile testing machine. Prior to the test, the specimen was preloaded with a preload of 1 N for 5 min. After preconditioning, the ultimate failure load was investigated with an elongation rate of 2 mm/min. The failure load was recorded from the load-displacement curve, and the stiffness was calculated from the slope of the curve. For each sample, the test was completed when the graft was ruptured or pulled out from the bone tunnel.

2.5. Statistical analysis

Data were expressed as mean ± standard deviation and analyzed using Graphpad Prism 7.0 statistical software (GraphPad Software, Inc.). The analysis of variance (ANOVA) or nonparametric Kruskal-Wallis test was performed according to the normality test to determine significant differences of measurement data among the three groups. $P < 0.05$ was considered to be significant.

3. Results

3.1. Characterization

SEM images revealed that the surface of fibers in PET group was smooth while the surface of fibers in the PET/BM-CaP and PET/ED-CaP groups became rough and many crystal particles deposited on the surface. The particles of the PET/ED-CaP group were more uniform than those of the PET/BM-CaP group (Fig. 1A). Qualitative analysis using EDS mapping showed that Ca, P and O ions were distributed on the PET fibers after CaP deposition (Fig. 1B). Notably, the Ca, P and O ions in the PET/ED-CaP group were more uniform on the surface as compared to the PET/BM-CaP group. Furthermore, the Ca/P ratio in the PET/BM-CaP group was 1.12/1, while it was 1.54/1 in PET/ED-CaP group, which was closer to the Ca/P ratio of hydroxyapatite (HA) (1.67/1).

TGA was used to examine the thermal properties of the PET/BM-CaP and PET/ED-CaP. From curves in Fig. 1C, it can be observed that at 700 °C, the weight percentages of residual weight were 3.96% and 24.11% for PET/BM-CaP and PET/ED-CaP, respectively. Moreover, the WCA of the PET/BM-CaP group (48.2° ± 2.2°) and the PET/ED-CaP group (47.1° ± 1.3°) was significantly smaller than that of the PET group (106.3° ± 1.1°) (both $P < 0.01$), indicating the hydrophilicity of PET was significantly improved after CaP deposition (Fig. 1D).

3.2. Cell attachment and proliferation

Calcein AM and propidium iodide were used to identify live and dead cells. As shown in Fig. 3A, the numbers of both live and dead cells increased over time in all three groups. The number and percentage of live cells in the PET/BM-CaP and PET/ED-CaP groups were significantly greater than that on the PET group after 5 days of culturing (Fig. 2A–B).

The attachment of MC3T3-E1 cells on PET, PET/BM-CaP and PET/ED-CaP scaffolds were observed by SEM (Fig. 2C). After 5 days of culturing, better cell spreading and more extracellular matrix secretion were observed in the PET/BM-CaP and PET/ED-CaP groups compared to the PET group. Besides, the level of cell proliferation was determined by CCK-8 cell counting (Fig. 2D). The cell proliferation in PET/BM-CaP group and PET group showed no significant difference at 1 day. However, at 3 and 5 days, the outcomes of PET/BM-CaP and PET/ED-CaP groups were significantly better than PET group (both $P < 0.01$), indicating the positive role of CaP deposition via BM or ED in cell proliferation.

3.3. Osteogenic differentiation and related signaling pathway of MC3T3-E1 cells

ALP activity was measured as an early marker of osteogenic differentiation. Fig. 3A showed the ALP staining in the PET/ED-CaP was stronger than that in the PET group and PET/BM-CaP group at 7 and 14 days. Meanwhile, the quantitative analysis revealed that ALP expression in the PET/ED-CaP group was significantly higher than that in the PET/BM-CaP group and PET group at 7 and 14 days, respectively (Fig. 3B). Besides, bone mineralization caused by calcium deposition was regarded as a late marker of osteogenic differentiation. Fig. 3C showed that ARS staining in the in the PET/ED-CaP group was stronger than that in the PET/BM-CaP group and PET group at 21 and 28 days. The quantitative analysis of the ARS revealed that the calcium nodule formation in the PET/ED-CaP group was significantly higher than that in the PET/BM-CaP group and PET group at days 21 and 28 days, respectively (Fig. 3D).

Moreover, the expression of osteogenesis-related genes, including ALP, COL1, OCN and OPN were detected by RT-qPCR. As shown in Fig. 4A, the expressions of ALP, COL1, OCN and OPN were significantly higher in the PET/BM-CaP group and PET/ED-CaP group compared to those in the PET group at 7 and 14 days (all $P < 0.01$). Meanwhile, PET/ED-CaP group also had higher expressions of ALP, COL1 and OPN at 7 days (all $P < 0.01$) and higher expressions of ALP, COL1, OCN and OPN at 14 days (all $P < 0.01$) compared to the PET/BM-CaP group.

To investigate the signaling pathway that may be involved in regulation of osteogenesis, Western blot was performed. As shown in Fig. 4B, a significant increase in the expressions of COL1, OPN, Wnt-5a and β-catenin was found in the PET/BM-CaP and PET/ED-CaP groups compared to the PET group at 7 days (all $P < 0.01$), suggesting CaP coating could activate β-catenin pathway for osteogenesis. The

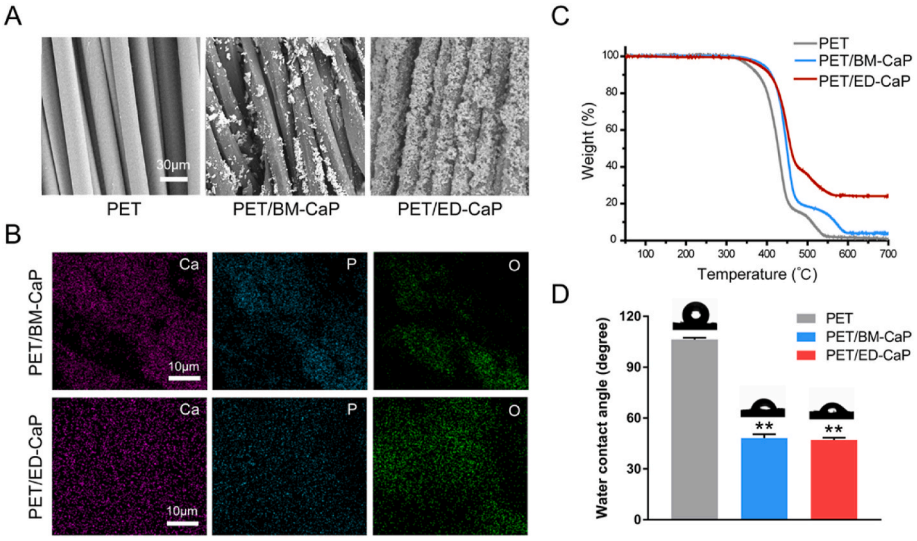

Fig. 1. (A) SEM morphology, (B) EDS mapping analysis, (C) TGA and (D) WCA measurements of PET, PET/BM-CaP and PET/ED-CaP fibers. **$P < 0.01$ compared to the PET group.

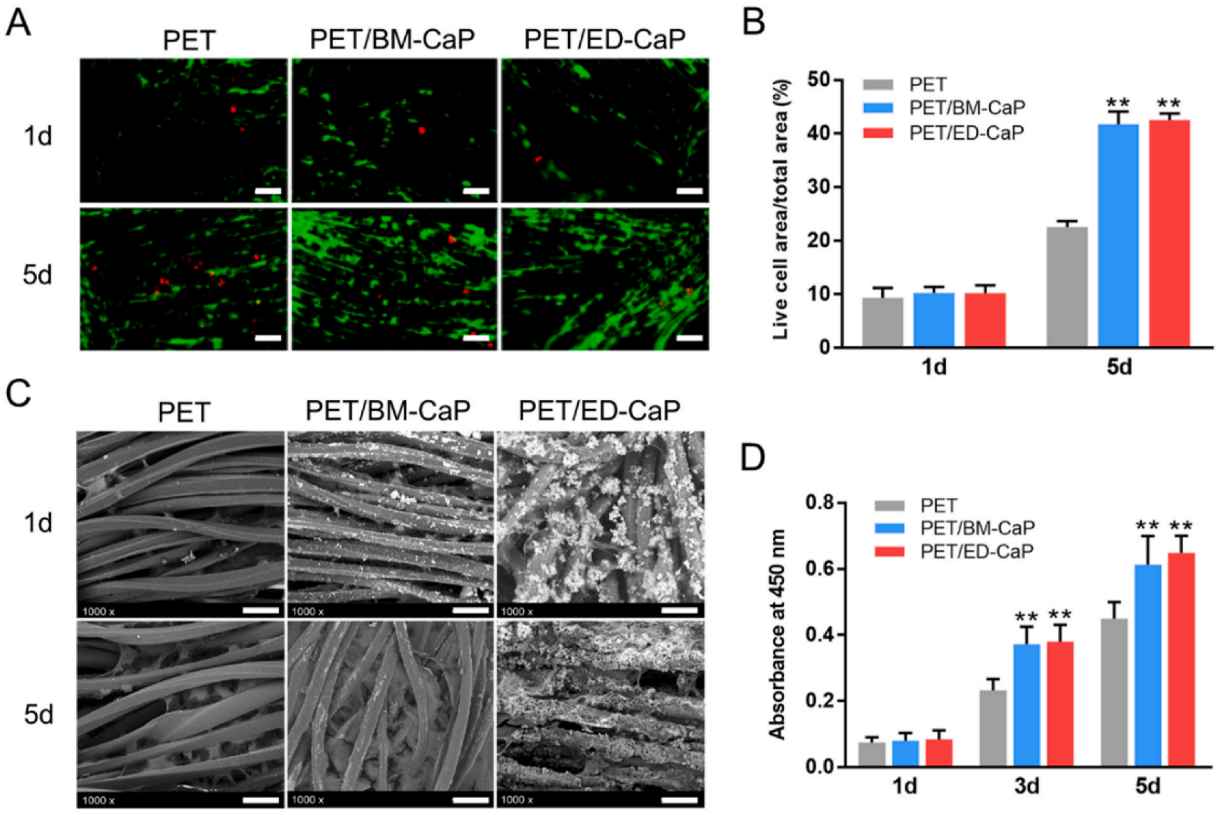

Fig. 2. The viability and SEM morphology of MC3T3-E1 in the PET, PET/BM-CaP and PET/ED-CaP groups. (A) Fluorescent images of live and dead cells staining after MC3T3-E1 cells cultured at 1 and 5 days on each scaffold. Scale bars = 100 μm. (B) Live cell area per total area analyzed from the fluorescent images of live and dead staining. (C) The SEM morphology of MC3T3-E1 cultured at 1 and 5 days on each scaffold. Scale bars = 40 μm. (D) CCK-8 assay of MC3T3-E1 cells cultured at 1, 3 and 5 days on each scaffold. **P < 0.01 compared to the PET group.

expressions of the COL1, OPN, Wnt-5a and β-catenin in the PET/ED-CaP were higher than those in the PET/BM-CaP (all P < 0.01), indicating PET/ED-CaP had best osteogenic effect *in vitro*.

3.4. Micro-CT analysis

The bone tunnels at 12 weeks were analyzed using micro-CT (Fig. 5). The mean areas of bone tunnels in the PET, PET/BM-CaP and PET/ED-CaP groups were 6.9 ± 0.4 mm^2, 5.1 ± 0.9 mm^2 and 4.0 ± 0.7 mm^2, respectively. The mean areas of bone tunnel in the PET/BM-CaP and PET/ED-CaP groups were much smaller than those of PET group (both P < 0.01). Furthermore, significant difference was also detected between PET/BM-CaP and PET/ED-CaP groups (P < 0.01). The BV/TV values in the PET, PET/BM-CaP and PET/ED-

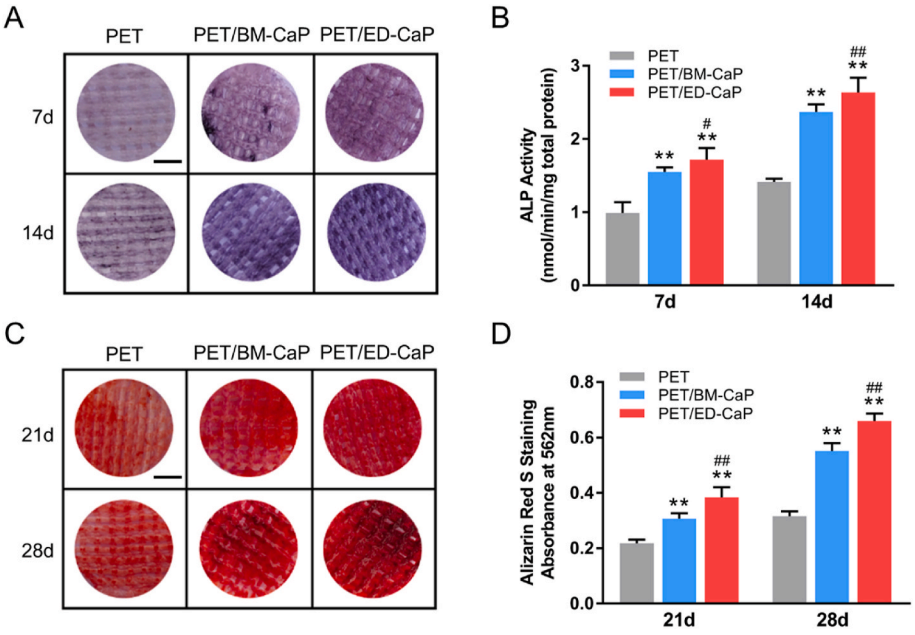

Fig. 3. Osteogenic differentiation evaluation of MC3T3-E1 in the PET, PET/BM-CaP and PET/ED-CaP groups. (A) ALP staining and (B) quantitative analysis of the MC3T3-E1 on each scaffold after osteogenic induction for 7 and 14 days. (C) ARS staining and (D) quantitative analysis of the MC3T3-E1 on each scaffold after osteogenic induction for 21 and 28 days. (A, C) Scale bars = 400 mm **P < 0.01 compared to the PET group; #P < 0.05 compared to the PET/BM-CaP group; ##P < 0.01 compared to the PET/BM-CaP group.

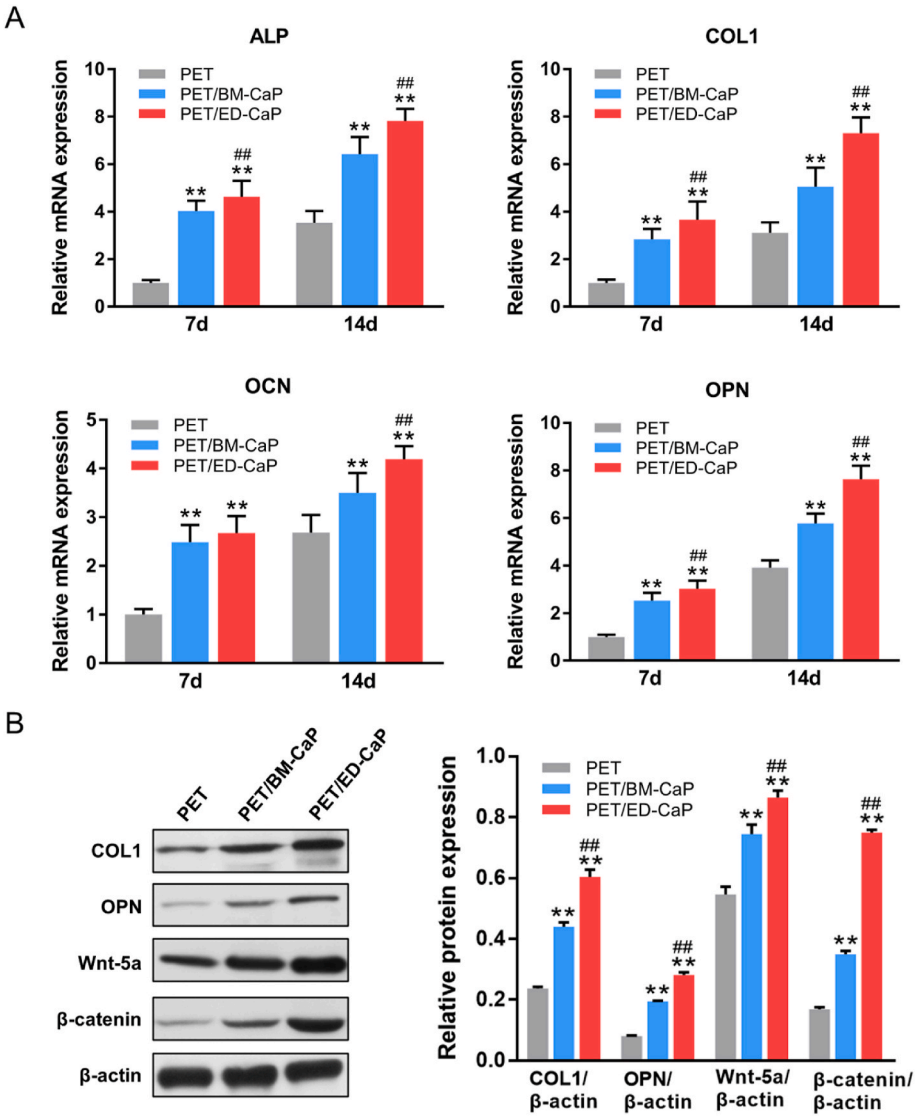

Fig. 4. (A) RT-qPCR for the relative mRNA expressions of ALP, COL1, OCN and OPN of MC3T3-E1 cells in the PET, PET/BM-CaP and PET/ED-CaP groups at 7 and 14 days. (B) Western blot assay and semi-quantification for COL1, OPN, Wnt-5a and β-catenin expressions of MC3T3-E1 cells in the PET, PET/BM-CaP and PET/ED-CaP groups at 7 days. **P < 0.01 compared to the PET group; ##P < 0.01 compared to the PET/BM-CaP group.

CaP groups were 10.1 ± 1.6%, 14.3 ± 3.4% and 18.2 ± 4.4%, respectively. Similarly, the BV/TV values were much higher in the PET/BM-CaP and PET/ED-CaP groups compared to those in the PET group (P < 0.05, P < 0.01 respectively). The BT/TV value of PET/ED-CaP group was significantly higher than those of the PET/BM-CaP group (P < 0.05). These results indicated that ED-CaP had most positive effect on bone ingrowth around the graft.

3.5. Histological and immunohistochemical assessment

As shown in Fig. 6A–B, interface filled with fibrous tissue was observed between the bone tissue and the graft in all the three groups at 6 weeks. However, the interface width in the PET/ED-CaP group was smaller than that of the PET/BM-CaP and PET groups, which indicated a better bone ingrowth. At 12 weeks, the fibrous tissue at the interface became mature and still existed in the PET group. However, there was new bone tissue instead of fibrous tissue growing into the graft in the PET/BM-CaP and PET/ED-CaP groups. Besides, the amount of new bone was larger in the PET/ED-CaP group than the PET/BM-CaP group. More importantly, TB staining showed that the fibrocartilage tissue formation was only observed in the PET/ED-CaP group (Fig. 6C). Accordingly, the histological score of the PET/ED-CaP group at 12 weeks was highest among the three groups (Fig. S1).

Meanwhile, the immunohistochemical staining showed that both the PET/BM-CaP and PET/ED-CaP groups at 12 weeks exhibited highly positive staining of Wnt-5a and β-catenin at the interface, highly positive staining of OPN at the bone tissue, and highly positive staining of COL1 at and around the bone tissue (Fig. 7). Moreover, COL2, COL1, OPN, Wnt-5a and β-catenin were most strongly expressed in the PET/ED-CaP group.

3.6. Biomechanical test

No graft rupture occurred and all the ligaments were pulled out from the bone tunnel. The ultimate failure load and stiffness increased in all the three groups from 6 to 12 weeks after surgery (Fig. 8A). At 6 weeks, the ultimate failure load of the PET/BM-CaP (39.0 ± 6.3 N) and PET/ED-CaP (40.4 ± 10.5 N) groups were higher than that of the PET group (24.3 ± 6.7 N) (P < 0.05, P < 0.01 respectively). However, significant difference was not detected between the PET/BM-CaP (76.4 ± 6.3 N) and PET/ED-CaP (93.9 ± 6.7 N) groups until at 12 weeks (P < 0.01). Besides, the stiffness of the three groups did not

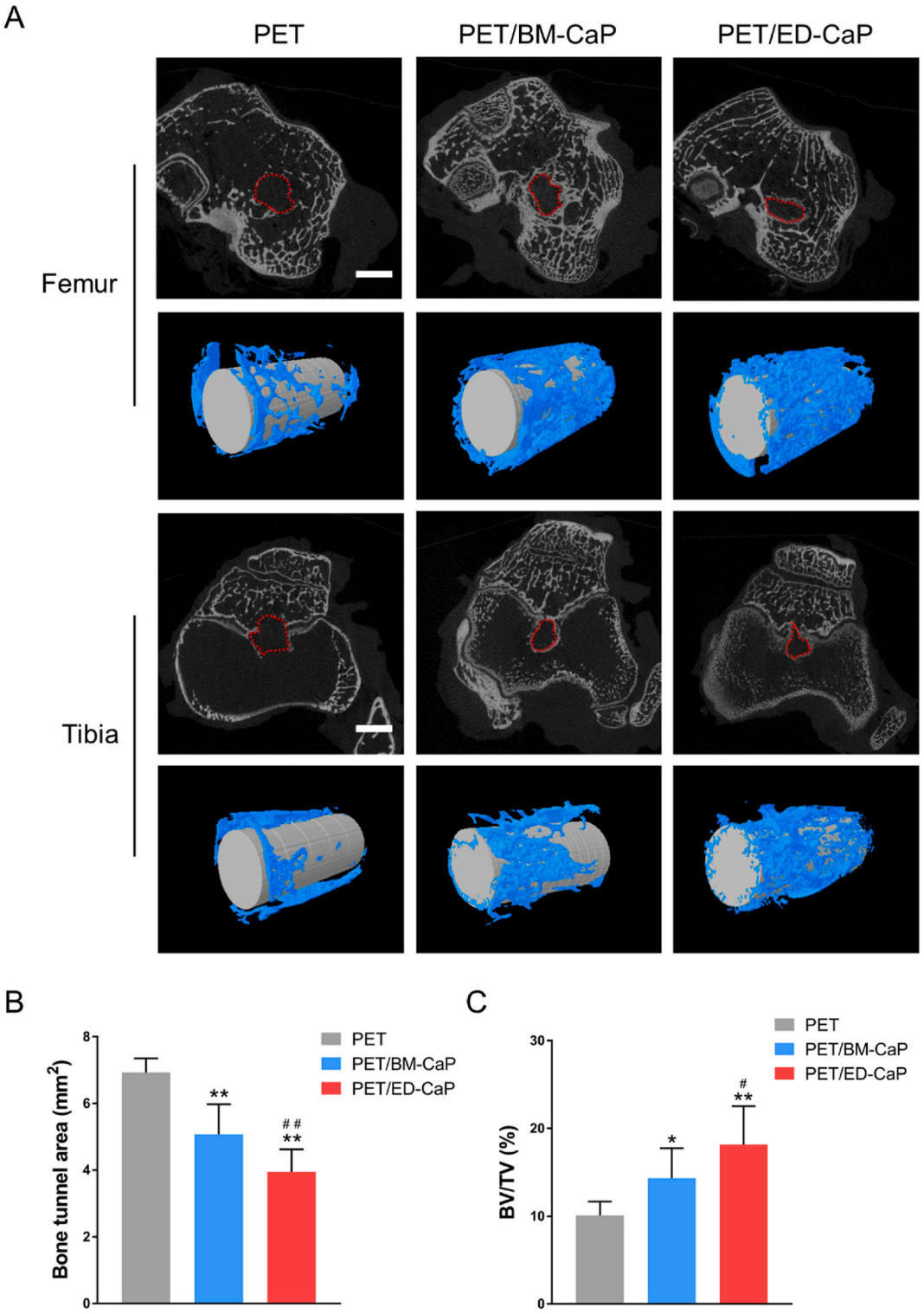

Fig. 5. Micro-CT analysis of the PET, PET/BM-CaP and PET/ED-CaP groups at 12 weeks after surgery. (A) The cross-sectional areas of the femur and tibial bone tunnels were measured and the three-dimensional (3D) images were reconstructed. (B) Quantitative analysis of cross-sectional bone tunnel areas. (C) Quantitative analysis of the BV/TV value. Scale bars = 3 mm *P < 0.05 compared to the PET group; **P < 0.01 compared to the PET group; #P < 0.05 compared to the PET/BM-CaP group; ##P < 0.01 compared to the PET/BM-CaP group.

display any significant difference until at 12 weeks (Fig. 8B). The stiffness in the PET/BM-CaP (15.8 ± 2.5 N/mm) and PET/ED-CaP (23.1 ± 3.9 N/mm) groups were significantly higher than that in the PET group (10.2 ± 2.3 N/mm) (both P < 0.01) (Fig. 8C). In addition, there was a significant difference of stiffness between the PET/BM-CaP and PET/ED-CaP groups (P < 0.05).

4. Discussion

The technique of CaP deposition onto PET ligament surface is a potential choice to facilitate graft-bone integration. Several studies have investigated the material characterization and the biological performance of CaP-based surface modification for PET ligament

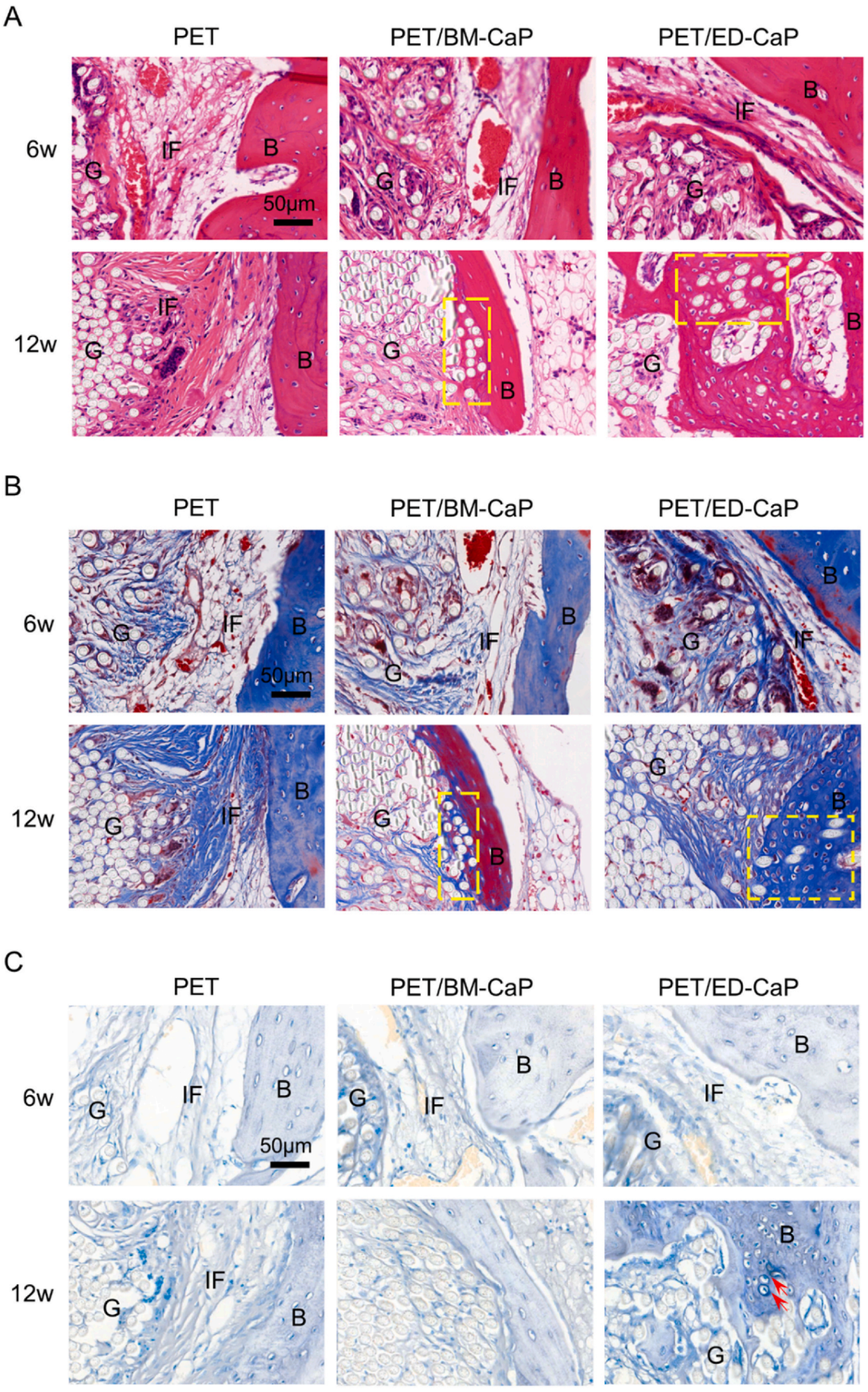

(caption on next page)

Fig. 6. (A) H&E, (B) Masson and (C) TB staining results of pathological sections in the PET, PET/BM-CaP and PET/ED-CaP groups at 6 and 12 weeks after surgery. New bone tissues grew into the graft (yellow rectangles) in the PET/BM-CaP and PET/ED-CaP groups at 12 weeks. Fibrocartilage tissue formed at the interface (red arrows) in the PET/ED-CaP group at 12 weeks. G, graft; B, bone; IF, interface. (For interpretation of the references to colour in this figure legend, the reader is referred to the Web version of this article.)

[13,19,20]. However, more studies are still needed to focus on how to give full play to the biological effect of CaP. In the present study, we compared the effect of PET ligament modified with ED and BM methods *in vitro* and *in vivo*, and demonstrated the superiority of ED-CaP based surface modification.

The deposition of CaP on the surface of PET scaffolds can be achieved via either BM or ED method. However, there were dramatic differences in the preparation and characterization of the scaffolds. For one thing, the deposition of CaP on the surface of PET fibers took only 2 h using the ED method, whereas it took more time using the BM method. For another, TGA exhibited that increased amount of CaP with Ca/P ratio closer to the HA was obtained on the PET/ED-CaP scaffold compared to the PET/BM-CaP scaffold. These results demonstrated that ED is a more efficient method for CaP deposition. Moreover, the BM method cannot uniform the CaP particles depositing on the surface of PET scaffolds, while the ED method was capable to achieve

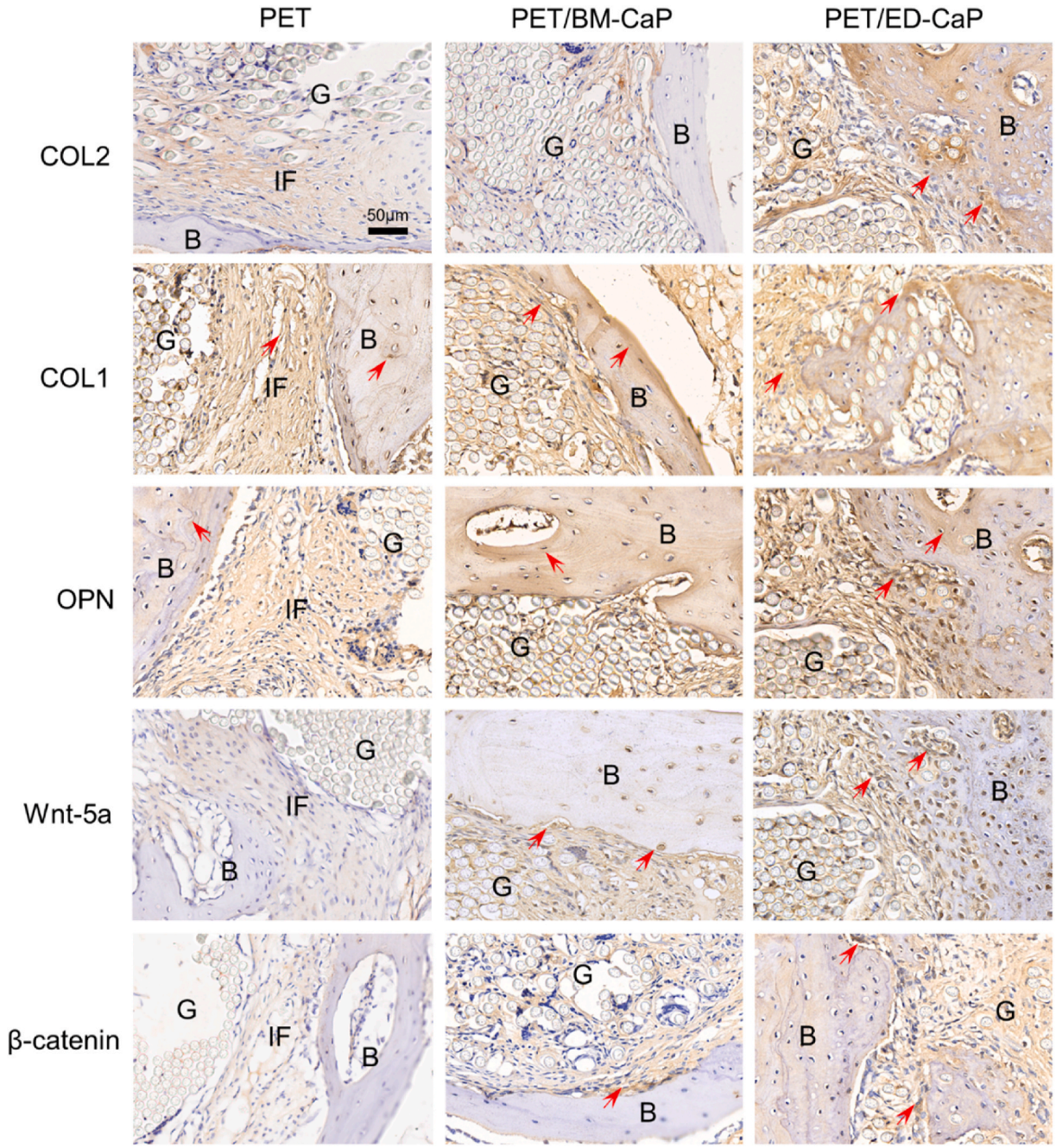

Fig. 7. Immunohistochemical staining results of COL2, COL1, OPN, Wnt-5a and β-catenin for the PET, PET/BM-CaP and PET/ED-CaP groups at 12 weeks after surgery. Red arrows indicate the positive staining tissues. G, graft; B, bone; IF, interface. (For interpretation of the references to colour in this figure legend, the reader is referred to the Web version of this article.)

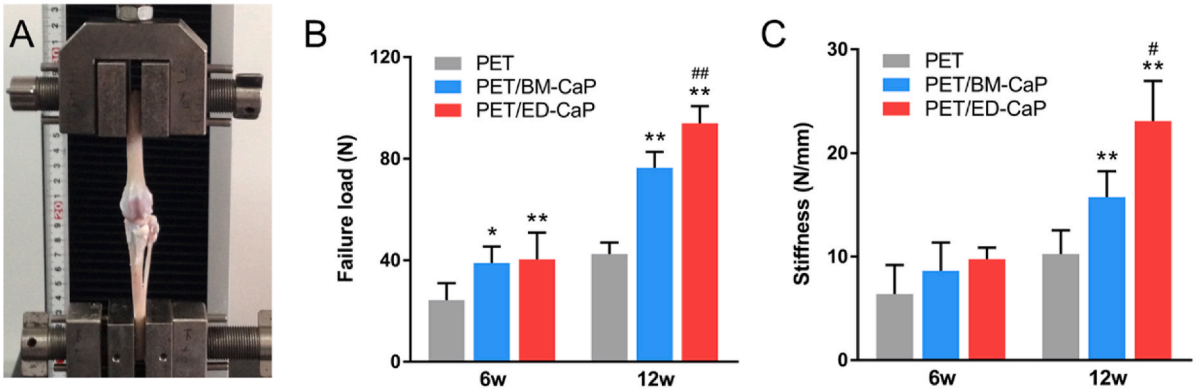

Fig. 8. Biomechanical test for specimens of the PET, PET/BM-CaP and PET/ED-CaP groups at 6 and 12 weeks after surgery. (A) Digital camera image of biomechanical test of a specimen. (B) Comparison of ultimate failure load among the three groups. (C) Comparison of stiffness among the three groups. *P < 0.05 compared to the PET group; **P < 0.01 compared to the PET group; #P < 0.05 compared to the PET/BM-CaP group; ##P < 0.01 compared to the PET/BM-CaP group.

homogeneous distribution of CaP particles on the surface of scaffold. This uniform topography of CaP particles in the PET/ED-CaP scaffold effectively avoided the shortcomings of random CaP particles, which might cause inflammatory reactions and slower bone formation [26,27]. Therefore, the PET/ED-CaP scaffolds may give full play to the bioactivity of CaP.

In vitro study showed that PET/BM-CaP and PET/ED-CaP scaffolds were capable of promoting MC3T3-E1 cells attachment and proliferation as compared to the PET scaffold. These results revealed the good cytocompatibility of CaP. Moreover, osteogenic differentiation of the MC3T3-E1 cells was stronger on the PET/ED-CaP scaffold than the PET/BM-CaP and PET scaffolds according to the results of ALP and ARS staining, RT-qPCR and Western blot. PET/ED-CaP scaffold had a larger amount of and more uniform CaP depositing on the surface, which lead to better osteogenic differentiation of the MC3T3-E1 cells. Bhattacharjee et al. [28] compared the osteogenic effect of different methods including co-electrospin, alternative soaking, and ED for introduction of nHA in the dual growth factor mediated silk fibroin grafted poly (ϵ-caprolactone) nanofibrous scaffolds. The authors found that the scaffolds with electrodeposited nHA most significantly promoted cell viability, ALP activity and osteogenesis-related genes expression levels of human mesenchymal stem cells, thus substantiating the superiority of ED. Besides, we observed that Wnt5a and β-catenin, which were known to play a role in the CaP-enhanced osteogenic differentiation [29], had highest expressions in Western blot and immunohistochemical staining of the PET/ED-CaP group. This indicated the Wnt/β-catenin signaling pathway might be involved in graft-bone integration induced by ED-CaP in our study.

It is well established that the healing potential of grafts in a bone tunnel is extremely poor due to an intervening layer of fibrovascular scar tissue between the graft and the bone [19]. This layer is poor in mechanical performance and becomes a “weak link” after surgical reconstruction [30]. In the present study, interface with a large amount of fibrous tissue was obviously observed in the PET group at 6 and 12 weeks, which lead to a poor ultimate failure load and stiffness according to the biomechanical test. On the contrast, there was new bone tissue instead of fibrous tissue growing into the graft in the PET/BM-CaP and PET/ED-CaP groups at 12 weeks, which conferred the mechanical strength. Therefore, the ultimate failure load and stiffness significantly increased in the PET/BM-CaP and PET/ED-CaP groups compared to the PET group.

More importantly, ED-CaP helped to generate not only new bone but also fibrocartilage tissues according to the histological results at 12 weeks, which contributed to the highest biomechanical property among the three groups. Previously, different methods such as dip coating, chemical grafting and pulsed laser deposition have been applied for surface modification of the PET ligament with several bioactive substances to enhance its bioactivity [18,20,31]. Yu et al. [31] chemically modified the PET artificial ligament with dopamine self-polymerization and then with mesoporous bioactive glass by sonication. Li et al. [18] reported copper containing bioactive glass nanocoating on the PET artificial ligament was successfully prepared by pulsed laser deposition. However, these methods did not induce a fibrocartilage structure between the graft and the bone. As this type of biomimetic tissue structure cannot be regenerated easily, the findings in our study could be of great significance. Schell et al. [32] reported that HA coating of the metallic osteochondral plug led to a better contact between implant and neighbouring bone as well as cartilage tissue for the osteochondral defect of sheep. The author noted that HA might have chondro-inductive quality in some condition *in vivo*. Mutsuzaki et al. [33] deposited CaP onto the autograft for ACL reconstruction of goats and also found a small fibrocartilage layer at the interface after 26 weeks postoperatively. We suppose that the CaP can induce direct bonding between the graft and bone. After direct bonding, the local mechanical environment of the graft-bone structure changes, as there is little graft-tunnel motion, which further induced chondrogenic differentiation of the interface tissue to form fibrocartilage structure [34].

Our study is not without limitations and scope for further work. Firstly, we merely focused on the graft-bone integration in the intraosseous part but not the remodeling process in the intra-articular part of the artificial ligament, which needed further assessment. Secondly, regarding to the animal model, the time points set at 6 weeks and 12 weeks were relatively short. Hence, long-term effects should be evaluated. Lastly, considering the biomechanical properties of the samples were still inferior to the native ACL [35], the growth factors as well as seed cells can be incorporated into the PET/ED-CaP scaffold for a better outcome. However, our study provides a promising modification strategy for PET artificial ligament to promote graft-bone integration after ACL reconstruction.

5. Conclusions

In this study, BM or ED method was applied to modify PET ligament with CaP. The ED method was proved to be more efficient and can produce uniform surface topography compared to BM method. *In vitro* study demonstrated that PET/ED-CaP scaffold significantly stimulated the proliferation and facilitated osteogenic differentiation of MC3T3-E1 cells, in which the Wnt/β-catenin signaling pathway might be involved. Moreover, *in vivo* study of a rabbit ACL reconstruction model substantiated that PET/ED-CaP significantly promoted graft-bone

integration. Particularly, the PET/ED-CaP induced fibrocartilage tissue formation and numerous new bone tissue ingrowth into the interface, which was responsible for the best biomechanical property among three groups at 12 weeks. Therefore, the PET/ED-CaP artificial ligament displays a great potential application for clinical ACL reconstruction in the future.

CRediT authorship contribution statement

Jiangyu Cai: Investigation, Methodology, Data curation, Formal analysis, Writing - original draft, Funding acquisition. **Qianqian Zhang:** Investigation, Methodology, Data curation, Formal analysis, Writing - original draft, Funding acquisition. **Jiebo Chen:** Investigation, Visualization, Formal analysis. **Jia Jiang:** Investigation, Formal analysis, Funding acquisition. **Xiumei Mo:** Resources. **Chuanglong He:** Conceptualization, Supervision, Writing - review & editing, Project administration. **Jinzhong Zhao:** Funding acquisition, Conceptualization, Supervision, Writing - review & editing, Project administration.

Declaration of competing interest

The authors declare that they have no known competing financial interests or personal relationships that could have appeared to influence the work reported in this paper.

Acknowledgments

This study was supported by the National Key Research and Development Program of China (Grant No. 2018YFC1106200 and 2018YFC1106202), the National Natural Science Foundation of China (Grant No. 81871753 and 81772341), China Postdoctoral Science Foundation (Grant No. 2020M671154), the Fundamental Research Funds for the Central Universities and Graduate Student Innovation Fund of Donghua University (Grant No. CUSF-DH-D-2019070).

Appendix A. Supplementary data

Supplementary data to this article can be found online at https://doi.org/10.1016/j.bioactmat.2020.08.037.

References

[1] C. Yilgor, P. Yilgor Huri, G. Huri, Tissue engineering strategies in ligament regeneration, Stem Cell. Int. 2012 (2012) 374676.
[2] J. Cai, L. Zhang, J. Chen, S. Chen, Silk fibroin coating through EDC/NHS crosslink is an effective method to promote graft remodeling of a polyethylene terephthalate artificial ligament, J. Biomater. Appl. 33 (2019) 1407–1414.
[3] F.A. Petrigliano, D.R. McAllister, B.M. Wu, Tissue engineering for anterior cruciate ligament reconstruction: a review of current strategies, Arthrosc. J. Arthrosc. Relat. Surg. 22 (2006) 441–451.
[4] D.P. Iliadis, D.N. Bourlos, D.S. Mastrokalos, E. Chronopoulos, G.C. Babis, LARS artificial ligament versus ABC purely polyester ligament for anterior cruciate ligament reconstruction, Orthop. J. Sport. Med. 4 (2016) 2325967116653359.
[5] H. Pauly, D. Kelly, K. Popat, J. Easley, R. Palmer, T.L. Haut Donahue, Mechanical properties of a hierarchical electrospun scaffold for ovine anterior cruciate ligament replacement, J. Orthop. Res. 37 (2019) 421–430.
[6] Q. Dong, J. Cai, H. Wang, S. Chen, Y. Liu, J. Yao, Z. Shao, X. Chen, Artificial ligament made from silk protein/Laponite hybrid fibers, Acta Biomater. 106 (2020) 102–113.
[7] S. Wu, R. Zhou, F. Zhou, P.N. Streubel, S. Chen, B. Duan, Electrospun thymosin Beta-4 loaded PLGA/PLA nanofiber/microfiber hybrid yarns for tendon tissue engineering application, Mater. Sci. Eng. C 106 (2020) 110268.
[8] S. Wu, Y. Wang, P.N. Streubel, B. Duan, Living nanofiber yarn-based woven biotextiles for tendon tissue engineering using cell tri-culture and mechanical stimulation, Acta Biomater. 62 (2017) 102–115.
[9] X. Jiang, S. Wu, M. Kuss, Y. Kong, W. Shi, P.N. Streubel, T. Li, B. Duan, 3D printing of multilayered scaffolds for rotator cuff tendon regeneration, Bioact. Mater. 5 (2020) 636–643.
[10] T. Chen, P. Zhang, J. Chen, Y. Hua, S. Chen, Long-term outcomes of anterior cruciate ligament reconstruction using either synthetics with remnant preservation or hamstring autografts: a 10-year longitudinal study, Am. J. Sports Med. 45 (2017) 2739–2750.
[11] T.M. Tiefenboeck, E. Thurmaier, M.M. Tiefenboeck, R.C. Ostermann, J. Joestl, M. Winnisch, M. Schurz, S. Hajdu, M. Hofbauer, Clinical and functional outcome after anterior cruciate ligament reconstruction using the LARS™ system at a minimum follow-up of 10 years, Knee 22 (2015) 565–568.
[12] J. Cai, J. Wang, K. Ye, D. Li, C. Ai, D. Sheng, W. Jin, X. Liu, Y. Zhi, J. Jiang, Dual-layer aligned-random nanofibrous scaffolds for improving gradient microstructure of tendon-to-bone healing in a rabbit extra-articular model, Int. J. Nanomed. 13 (2018) 3481–3492.
[13] H. Li, S. Chen, J. Chen, J. Chang, M. Xu, Y. Sun, C. Wu, Mussel-inspired artificial grafts for functional ligament reconstruction, ACS Appl. Mater. Interfaces 7 (2015) 14708–14719.
[14] Y.J. No, M. Castilho, Y. Ramaswamy, H. Zreiqat, Role of biomaterials and controlled architecture on tendon/ligament repair and regeneration, Adv. Mater. 1904511 (2019) 1–16.
[15] H. Li, S. Chen, Biomedical coatings on polyethylene terephthalate artificial ligaments, J. Biomed. Mater. Res. 103 (2015) 839–845.
[16] C.H. Wang, Z.S. Guo, F. Pang, L.Y. Zhang, M. Yan, J.H. Yan, K.W. Li, X.J. Li, Y. Li, L. Bi, Y.S. Han, Effects of graphene modification on the bioactivation of polyethylene-terephthalate-based artificial ligaments, ACS Appl. Mater. Interfaces 7 (2015) 15263–15276.
[17] S. Wang, Y. Ge, C. Ai, J. Jiang, J. Cai, D. Sheng, F. Wan, X. Liu, Y. Hao, J. Chen, Enhance the biocompatibility and osseointegration of polyethylene terephthalate ligament by plasma spraying with hydroxyapatite in vitro and in vivo, Int. J. Nanomed. 13 (2018) 3609–3623.
[18] H. Li, J. Li, J. Jiang, F. Lv, J. Chang, S. Chen, C. Wu, An osteogenesis/angiogenesis-stimulation artificial ligament for anterior cruciate ligament reconstruction, Acta Biomater. 54 (2017) 399–410.
[19] H. Li, Y. Ge, Y. Wu, J. Jiang, K. Gao, P. Zhang, L. Wu, S. Chen, Hydroxyapatite coating enhances polyethylene terephthalate artificial ligament graft osseointegration in the bone tunnel, Int. Orthop. 35 (2011) 1561–1567.
[20] J. Jiang, F. Wan, J. Yang, W. Hao, Y. Wang, J. Yao, Z. Shao, P. Zhang, J. Chen, L. Zhou, S. Chen, Enhancement of osseointegration of polyethylene terephthalate artificial ligament by coating of silk fibroin and depositing of hydroxyapatite, Int. J. Nanomed. 9 (2014) 4569–4580.
[21] C. He, G. Xiao, X. Jin, C. Sun, P.X. Ma, Electrodeposition on nanofibrous polymer scaffolds: rapid mineralization, tunable calcium phosphate composition and topography, Adv. Funct. Mater. 20 (2010) 3568–3576.
[22] W. Nie, Y. Gao, D.J. McCoul, G.J. Gillispie, Y.Z. Zhang, L. Liang, C.L. He, Rapid mineralization of hierarchical poly(L-lactic acid)/poly(ε-caprolactone) nanofibrous scaffolds by electrodeposition for bone regeneration, Int. J. Nanomed. 14 (2019) 3929–3941.
[23] Y.M. Li, J. Jiang, S.K. Dong, J.Z. Zhao, J.Y. Wu, H.Y. He, C.S. Liu, Y.S. Chen, Chondroitin sulfate-polydopamine modified polyethylene terephthalate with extracellular matrix-mimetic immunoregulatory functions for osseointegration, J. Mater. Chem. B. 7 (2019) 7756–7770.
[24] C. Ai, J. Cai, J. Zhu, J. Zhou, J. Jiang, S. Chen, Effect of PET graft coated with silk fibroin via EDC/NHS crosslink on graft-bone healing in ACL reconstruction, RSC Adv. 7 (2017) 51303–51312.
[25] P. Cheng, P. Han, C. Zhao, S. Zhang, H. Wu, J. Ni, P. Hou, Y. Zhang, J. Liu, H. Xu, S. Liu, X. Zhang, Y. Zheng, Y. Chai, High-purity magnesium interference screws promote fibrocartilaginous entheses regeneration in the anterior cruciate ligament reconstruction rabbit model via accumulation of BMP-2 and VEGF, Biomaterials 81 (2016) 14–26.
[26] M. Prakasam, J. Locs, K. Salma-Ancane, D. Loca, A. Largeteau, L. Berzina-Cimdina, Fabrication, properties and applications of dense hydroxyapatite: a review, J. Funct. Biomater. 6 (2015) 1099–1140.
[27] C.C. Ribeiro, C.C. Barrias, M.A. Barbosa, Preparation and characterisation of calcium-phosphate porous microspheres with a uniform size for biomedical applications, J. Mater. Sci. Mater. Med. 17 (2006) 455–463.
[28] P. Bhattacharjee, T.K. Maiti, D. Bhattacharya, S.K. Nandi, Effect of different mineralization processes on in vitro and in vivo bone regeneration and osteoblast-macrophage cross-talk in co-culture system using dual growth factor mediated non-mulberry silk fibroin grafted poly (Є-caprolactone) nanofibrous scaffold, Colloids Surf. B Biointerfaces 156 (2017) 270–281.
[29] Y. Wang, J. Pan, Y. Zhang, X. Li, Z. Zhang, P. Wang, Z. Qin, J. Li, Wnt and Notch signaling pathways in calcium phosphate-enhanced osteogenic differentiation: a pilot study, J. Biomed. Mater. Res. B Appl. Biomater. 107 (2019) 149–160.
[30] W. Zhai, C. Lv, Y. Zheng, Y. Gao, Z. Ding, Z. Chen, Weak link of tendon-bone healing and a control experiment to promote healing, Arch. Orthop. Trauma Surg. 133 (2013) 1533–1541.
[31] B. Yu, P. Pei, B. Yu, D. Li, X. Zhang, J. Huang, H. Ding, S. Chen, Y. Zhu, Enhance the bioactivity and osseointegration of the polyethylene-terephthalate-based artificial ligament via poly(dopamine) coating with mesoporous bioactive glass, Adv. Eng. Mater. 19 (2017).
[32] H. Schell, E. Zimpfer, K. Schmidt-Bleek, T. Jung, G.N. Duda, L. Ryd, Treatment of osteochondral defects: chondrointegration of metal implants improves after hydroxyapatite coating, Knee Surgery, Sport, Traumatol. Arthrosc. 27 (2019) 3575–3582.
[33] H. Mutsuzaki, H. Fujie, H. Nakajima, M. Fukagawa, S. Nomura, M. Sakane, Effect of calcium phosphate–hybridized tendon graft in anatomic single-bundle ACL reconstruction in goats, Orthop. J. Sport. Med. 4 (2016) 1–8.
[34] S.A. Rodeo, S. Kawamura, H.-J. Kim, C. Dynybil, L. Ying, Tendon healing in a bone tunnel differs at the tunnel entrance versus the tunnel exit: an effect of graft-tunnel motion? Am. J. Sports Med. 34 (2006) 1790–1800.
[35] G.J. Rogers, B.K. Milthorpe, A. Muratore, K. Schindhelm, Measurement of the mechanical properties of the ovine anterior cruciate ligament bone-ligament-bone complex: a basis for prosthetic evaluation, Biomaterials 11 (1990) 89–96.